

# Synthesis of Nitrogen-doped Carbon Nanotubes with Layered Double Hydroxides Containing Iron, Cobalt or Nickel as Catalyst Precursors

Yong Cao<sup>a,b</sup>, Qingze Jiao<sup>b</sup>, Yun Zhao<sup>b,\*</sup>, Gangfu Song<sup>a</sup> and Peiyong Zhang<sup>a</sup>

<sup>a</sup>Institute of Environment and Municipal Engineering, North China Institute of Water Conservancy and Hydroelectric Power, Zhengzhou 450011, People's Republic of China.

<sup>b</sup>School of Chemical Engineering and the Environment, Beijing Institute of Technology, Beijing 100081, People's Republic of China.

Received 31 March 2009, revised 13 April 2010, accepted 7 May 2010.

## ABSTRACT

Nitrogen-doped carbon nanotubes (CN<sub>x</sub>) were synthesized by the catalytic chemical vapour deposition of ethylenediamine with layered double hydroxides (LDHs) containing iron, cobalt or nickel as catalyst precursors at 650 °C. The catalytically active metal particles were obtained by calcination of LDHs followed by reduction. X-ray diffraction was used to characterize the structures of the precursors and their calcined products. Transmission electron microscopy, X-ray photoelectron spectroscopy and Raman spectroscopy were used to characterize the grown CN<sub>x</sub>. The results show that the CN<sub>x</sub> grown with Mg<sub>2</sub>Fe-LDH as catalyst precursor have a bamboo-like morphology and large diameter, while hollow tubes are obtained with CoMgAl- and NiMgAl-LDH as catalyst precursors. The CN<sub>x</sub> grown with CoMgAl-LDH have the highest N-doped content and the CN<sub>x</sub> grown with NiMgAl-LDH have the highest degree of graphitization among these three products.

## KEYWORDS

N-doped carbon nanotubes, layered double hydroxides, chemical vapour deposition.

## 1. Introduction

Layered double hydroxides (LDHs) are composed of charged brucite-like layers of divalent and trivalent metal hydroxides, whose excess positive charge due to the incorporated trivalent metal cation is balanced by anions in the interlayer.<sup>1</sup> Highly dispersed metal nanoparticles over oxide matrices can be obtained by simply designing an appropriate LDH precursor containing the desired catalytically active metal cations and by calcining the LDHs and further reducing the calcined LDHs in a controlled manner. This is possible due to the ordered prearrangement of metal cations in the layers of LDH precursor at an atomic level. For instance, Zhao *et al.*<sup>2</sup> have recently synthesized carbon nanostructures (nanofibres, single-walled and multi-walled carbon nanotubes) with Fe<sub>0.1</sub>Mg<sub>2</sub>Al<sub>0.9</sub>-, Fe<sub>0.1</sub>Zn<sub>2</sub>Al<sub>0.9</sub>- and Fe<sub>0.1</sub>Cu<sub>2</sub>Al<sub>0.9</sub>-LDH as catalyst precursors at 910 °C.

Altering the physico-chemical properties of carbon nanotubes (CNTs) has become an important topic in nanotechnology as their possibilities for application expand, for example as electronic devices,<sup>3–5</sup> catalyst support materials<sup>6–8</sup> or solid base catalysts<sup>9</sup>. This can be achieved by changing the local electron density in these materials by substituting C with heteroatoms such as N in the graphite sheets that form CNTs. Various methods have been applied to incorporate N into CNTs.<sup>9–21</sup> Among these are magnetron sputtering,<sup>12</sup> laser ablation,<sup>13</sup> pyrolysis of mixtures of organometallic- and N-containing organic compounds<sup>14–17</sup> and chemical vapour deposition (CVD) of N-containing hydrocarbons over heterogeneous iron, cobalt or nickel catalysts.<sup>9,18–21</sup>

In this paper, we synthesized the CN<sub>x</sub> by catalytic CVD of ethylenediamine with CoMgAl-, NiMgAl- and Mg<sub>2</sub>Fe-LDH as catalyst precursors at 650 °C. The effect of catalyst on morphology, N-doped content, distribution of different N structures and the degree of graphitization of CN<sub>x</sub> was investigated.

## 2. Experimental

### 2.1. Preparation of Precursors

CoMgAl-, NiMgAl- and Mg<sub>2</sub>Fe-LDH were prepared using a coprecipitation reaction. A solution containing Mg(NO<sub>3</sub>)<sub>2</sub>·6H<sub>2</sub>O and Fe(NO<sub>3</sub>)<sub>3</sub>·9H<sub>2</sub>O (Mg/Fe molar ratio = 2), Ni(NO<sub>3</sub>)<sub>2</sub>·6H<sub>2</sub>O, Mg(NO<sub>3</sub>)<sub>2</sub>·6H<sub>2</sub>O and Al(NO<sub>3</sub>)<sub>3</sub>·9H<sub>2</sub>O (Ni/Mg/Al molar ratio = 1/1/1) or Co(NO<sub>3</sub>)<sub>2</sub>·6H<sub>2</sub>O, Mg(NO<sub>3</sub>)<sub>2</sub>·6H<sub>2</sub>O and Al(NO<sub>3</sub>)<sub>3</sub>·9H<sub>2</sub>O (Co/Mg/Al molar ratio = 1/1/1) was added, slowly and with vigorous stirring, to another solution containing NaOH and Na<sub>2</sub>CO<sub>3</sub> {n(NaOH)/[n(M<sup>2+</sup>) + n(M<sup>3+</sup>)] = 1.6, n(CO<sub>3</sub><sup>2-</sup>)/n(M<sup>3+</sup>) = 2}. The resulting slurry was aged for 1 h at 90 °C. The final precipitate was filtered, washed thoroughly with water and dried.

The mixed oxides were obtained by calcination of LDH precursors at 600 °C for 4 h in air.

### 2.2. Synthesis of CN<sub>x</sub>

About 0.20 g of mixed oxide was loaded in a quartz boat and placed in the middle of a horizontal furnace, which was heated under flowing Ar (200 mL min<sup>-1</sup>) at a rate of 5 °C min<sup>-1</sup>. On reaching 400 °C, Ar was switched to H<sub>2</sub> (120 standard mL min<sup>-1</sup>) to reduce the mixed metal oxide. On reaching 650 °C, ethylenediamine was pumped into the furnace at a rate of 0.2 mL min<sup>-1</sup> in a mixture of Ar and H<sub>2</sub> (Ar, 400 mL min<sup>-1</sup>; H<sub>2</sub>, 100 standard mL min<sup>-1</sup>). The reaction was maintained for about 30 min, after which the furnace was allowed to cool to room temperature under Ar. The products grown with CoMgAl-, NiMgAl- and Mg<sub>2</sub>Fe-LDH as precursors were labelled CN<sub>x</sub>-Co, CN<sub>x</sub>-Ni and CN<sub>x</sub>-Fe, respectively.

Purification was achieved by refluxing the as-prepared products in a dilute nitric acid solution (30 % HNO<sub>3</sub>) at 60 °C for 8 h.

\* To whom correspondence should be addressed. E-mail: zhaoyun@bit.edu.cn

### 2.3. Techniques of Characterization

The catalysts were characterized by X-ray diffraction (XRD, X'PERT PRO MPD X-ray diffractometer, PANalytical, Inc., Almelo, the Netherlands) using  $\text{CuK}\alpha_1$  radiation. The generator tension was 40 kV and the generator current was 40 mA. Transmission electron microscopy (TEM), X-ray photoelectron spectroscopy (XPS) and Raman spectroscopy were used to characterize the purified tubes. The morphology of  $\text{CN}_x$  nanotubes was examined by TEM using a JEM-1200EX electron microscope (JEOL, Ltd., Tokyo, Japan). The purified  $\text{CN}_x$  nanotubes were suspended in ethanol and a drop of the suspension was deposited on a copper grid and the solvent was evaporated. Micrographs were taken at 100 kV. The content and the structure of N in  $\text{CN}_x$  nanotubes was determined by XPS (Physical Electronics PHI 5300, Perkin-Elmer, Inc., Waltham, MA, USA) using a vacuum generators XPS system operating with  $\text{MgK}\alpha$  radiation. The raw data were corrected for charging using the binding energy of graphite at 284.6 eV. Peak areas were determined after background subtraction using Shirley's method and fitting the spectra with Gaussian curves. The content of N incorporated was calculated from the peak areas of the C1s and N1s peaks after correcting for differences in sensitivity using sensitivity factors of 0.25 and 0.42 for C and N, respectively. Raman spectroscopy was carried out on a Renishaw Via-Reflex instrument (Renishaw, Wotton-under-Edge, Glos., UK) using an excitation wavelength of 532 nm.

## 3. Results and Discussion

### 3.1. XRD Characterization of LDHs and their Calcined Products

Figures 1 (a), (b) and (c) show XRD patterns for as-prepared  $\text{Mg}_2\text{Fe}$ -,  $\text{NiMgAl}$ - and  $\text{CoMgAl}$ -LDH. All the XRD patterns exhibit the characteristic reflections of a LDH material, which show that it contains hydroxylated as the main component, exhibiting sharp and symmetric reflections at low angle corresponding to the basal spacing and higher order reflections. Other crystalline phases were not detected. After calcination (Fig. 2 (a), (b) and (c)), the characteristic reflections corresponding to the layered structure of LDH disappeared and new reflections appeared. In Fig. 2 (a), new reflections indicate the presence of  $\text{MgO}$  (JCPDS, No. 75-0447),  $\text{Fe}_2\text{O}_3$  (JCPDS, No. 84-0307) and  $\text{MgFe}_2\text{O}_4$  (JCPDS, No. 01-1120). It is difficult to distinguish the different phases in Fig. 2 (b) due to the superposition of characteristic reflections of  $\text{MgO}$  (JCPDS, No. 75-0447) and  $\text{NiO}$  (JCPDS, No. 78-0643). In Fig. 2 (c), new reflections indicate the presence of  $\text{Co}_3\text{O}_4$  (JCPDS, No. 74-2120),  $\text{MgAl}_2\text{O}_4$  (JCPDS, No. 82-2424) and  $\text{CoAl}_2\text{O}_4$  (JCPDS, No. 82-2252). The use of LDH precursors with uniformly distributed cations seems to facilitate formation of spinel phases.<sup>22</sup> Co (or Mg) and Al (or Fe) mixed oxides usually lead to normal spinels, where  $\text{Co}^{2+}$  (or  $\text{Mg}^{2+}$ ) occupies tetrahedral sites and  $\text{Al}^{3+}$  (or  $\text{Fe}^{3+}$ ) fills in the octahedral positions. So the presence of spinels such as  $\text{MgFe}_2\text{O}_4$ ,  $\text{CoAl}_2\text{O}_4$  and  $\text{MgAl}_2\text{O}_4$  in the calcined LDHs is expected.

### 3.2. Characterization of $\text{CN}_x$

TEM images of the  $\text{CN}_x$  grown with various catalysts are shown in Fig. 3. The  $\text{CN}_x$  diameters of  $\text{CN}_x\text{-Co}$  (Fig. 3 (a)) and  $\text{CN}_x\text{-Ni}$  (Fig. 3 (b)) are about 25 nm, while they are about 20–50 nm for  $\text{CN}_x\text{-Fe}$  (Fig. 3 (c)). Almost all  $\text{CN}_x\text{-Fe}$  have an obvious bamboo-like morphology with transverse carbon bridges forming compartments, similar to other reported structures of  $\text{CN}_x$ .<sup>9–13</sup> For  $\text{CN}_x\text{-Ni}$  and  $\text{CN}_x\text{-Co}$ , the bamboo-like morphology is not obvious. This phenomenon has been

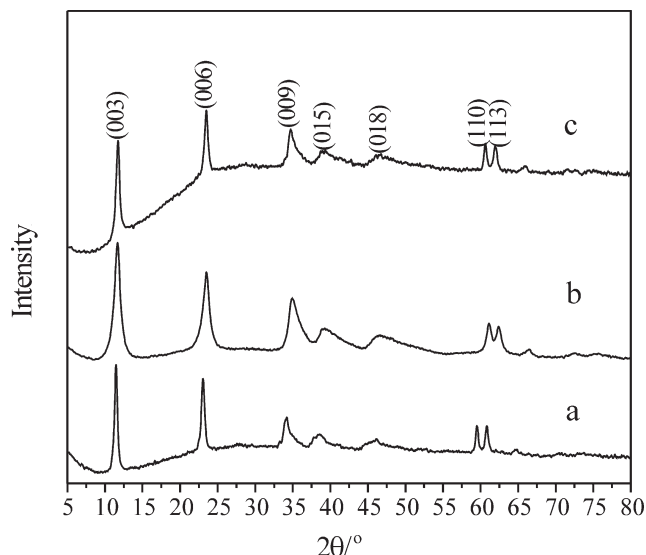


**Figure 1** Powder XRD patterns for as-prepared (a)  $\text{Mg}_2\text{Fe}$ -LDH; (b)  $\text{NiMgAl}$ -LDH; and (c)  $\text{CoMgAl}$ -LDH.

reported previously.<sup>23</sup> A possible explanation for the different morphology results from the difference in thermodynamic stabilities of the metal carbides. As Fe carbides are more stable than Co and Ni carbides,<sup>24</sup> a higher carbon concentration likely exists at the Fe surface as well as in the bulk. This means that the chance of forming a graphitic envelope around Fe is higher than for Co or Ni carbides, which causes the growth of CNTs on an Fe surface to be more pulsating as opposed to a more continuous growth, as in the case of Co or Ni.

XPS analysis was carried out on the  $\text{CN}_x$  grown with various catalysts to determine the content and structure of N in each product. The C1s and N1s XPS spectra of  $\text{CN}_x$  nanotubes are displayed in Figs. 4 (A) and (B), respectively. All XPS spectra show that the tubes consist of C accompanied by small amounts of N. The N-doped content, which was defined as the  $\text{N}/(\text{N}+\text{C})$  atomic % ratio, was estimated by the area ratio of the C1s and N1s peaks, taking into consideration their relative sensitivities.

For all XPS spectra, the asymmetric C1s band and N1s band can be observed centered at 284.6 eV and 401.1 eV. From the curve fitting, the N1s band can be deconvoluted into two bands at

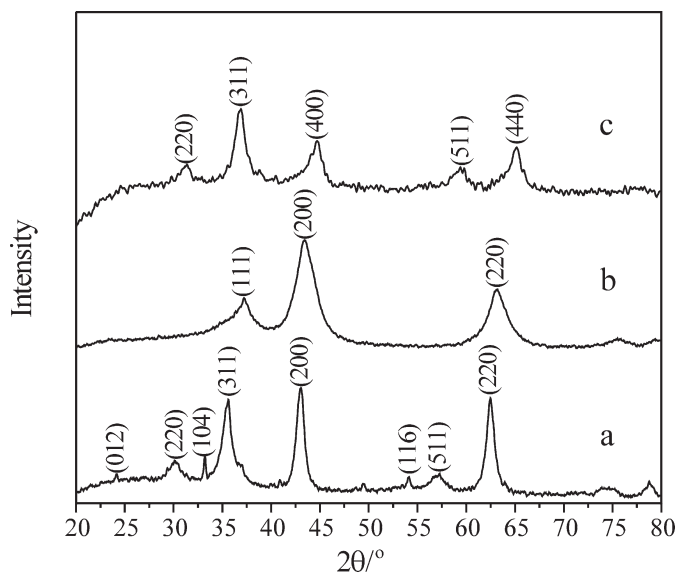


**Figure 2** Powder XRD patterns for calcined (a)  $\text{Mg}_2\text{Fe}$ -LDH; (b)  $\text{NiMgAl}$ -LDH; and (c)  $\text{CoMgAl}$ -LDH.

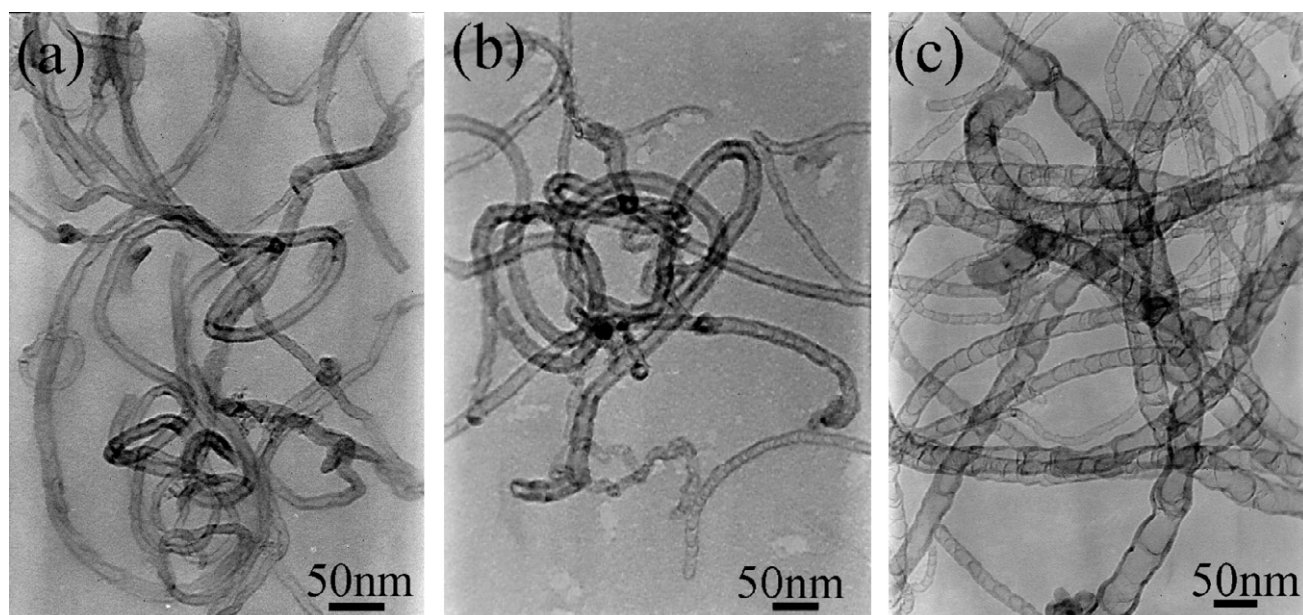


Figure 3 TEM micrographs of (a)  $\text{CN}_x\text{-Co}$ ; (b)  $\text{CN}_x\text{-Ni}$ ; and (c)  $\text{CN}_x\text{-Fe}$ .

around 399.5 eV (PN1) and 401.8 eV (PN2). The PN1 and PN2 bands correspond to pyridine-like and graphitic-like N.<sup>11,17</sup> The pyridine-like N correspond to the N atoms that contribute to the system with a pair of electrons, whereas graphitic-like N correspond to the N atoms substituting for C atoms in the graphite layers.<sup>13</sup> There are several ways in which N can be incorporated in the CNT lattice.<sup>18</sup> However, there are only two ways observed in our studies, as reported by others.<sup>11,17,19</sup> The N-doped content and intensity of PN1 and PN2 structures are listed in Table 1.  $\text{CN}_x\text{-Co}$  has the highest N-doped content of 7.4 atomic %, while  $\text{CN}_x\text{-Ni}$  has the highest PN1 content of these three products.

The Raman spectra of the  $\text{CN}_x$  grown with various catalysts are shown in Fig. 5. All spectra show mainly two bands at  $\sim 1350\text{ cm}^{-1}$  (D-band) and  $\sim 1580\text{ cm}^{-1}$  (G-band). The G band originates from the Raman active  $E_{2g}$  mode due to in-plane atomic displacements. The origin of the D band has been explained as a disorder-induced feature due to the finite particle size effect or lattice distortion.<sup>25</sup> It is known that the smaller ratio of  $I_D/I_G$  reflects the higher ordering of the graphite phase. The value of  $I_D/I_G$  for  $\text{CN}_x$  is also displayed in Table 1. The  $\text{CN}_x\text{-Ni}$  with  $I_D/I_G$  of 1.26 has the highest degree of graphitization among these three products. As

Table 1 XPS and Raman results of the grown  $\text{CN}_x$ .

Catalyst precursor	N-doped content/ atomic %	Relative intensities of N structures/%		$I_D/I_G$
		PN1	PN2	
CoMgAl-LDH	7.4	46	54	1.35
NiMgAl-LDH	5.5	49	51	1.26
Mg <sub>2</sub> Fe-LDH	6.3	38	62	1.61

$\text{CN}_x\text{-Fe}$  with a bamboo-like morphology has more defects and a higher degree of disorder than  $\text{CN}_x\text{-Co}$  with a hollow morphology, it can be expected that the  $I_D/I_G$  value of  $\text{CN}_x\text{-Fe}$  is higher than that of  $\text{CN}_x\text{-Co}$  although  $\text{CN}_x\text{-Co}$  has a higher N-doped content.

#### 4. Conclusions

$\text{CN}_x$  were synthesized by the catalytic CVD of ethylenediamine over LDHs containing iron, cobalt or nickel as catalyst precursors at 650 °C. The influence of catalyst on morphology, N-doped content, distribution of different N structures and the degree of graphitization of  $\text{CN}_x$  was studied. Almost all  $\text{CN}_x\text{-Fe}$

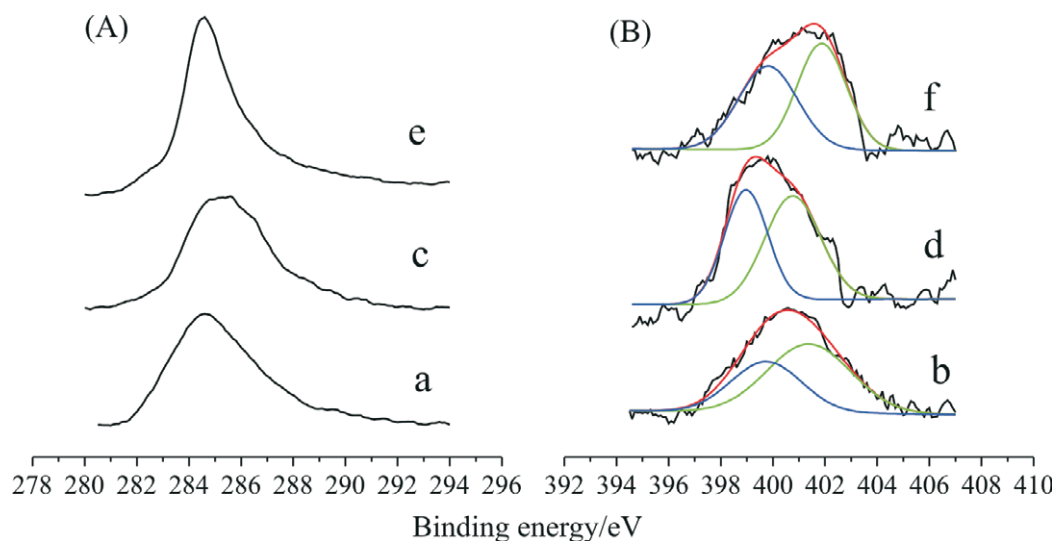


Figure 4 C1s (A) and N1s (B) XPS spectra of (a, b)  $\text{CN}_x\text{-Fe}$ ; (c, d)  $\text{CN}_x\text{-Ni}$ ; and (e, f)  $\text{CN}_x\text{-Co}$ .

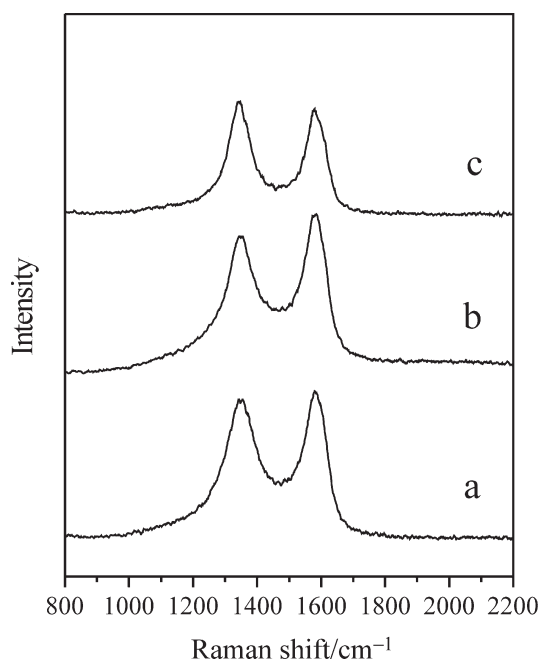


Figure 5 Raman spectra of (a)  $\text{CN}_x\text{-Fe}$ ; (b)  $\text{CN}_x\text{-Ni}$ ; and (c)  $\text{CN}_x\text{-Co}$ .

had a bamboo-like morphology with large diameter, while hollow tubes were obtained in  $\text{CN}_x\text{-Co}$  and  $\text{CN}_x\text{-Ni}$ . A possible explanation for the different morphology is due to the difference in thermodynamic stabilities of the metal carbides. Fe carbides are more stable compared with the Co and Ni carbides, which might result in a pulsating growth over Fe, while Co and Ni grow in a continuous way.  $\text{CN}_x\text{-Co}$  has the highest N-doped content (7.4 atomic %), while  $\text{CN}_x\text{-Ni}$  has the highest degree of graphitization and the most pyridine-like N structures among the three products.

#### Acknowledgements

This work was conducted with financial support from the Chinese National '863' (No. 2006AA03Z570) fund and Excellent Young Scholars Research Fund of Beijing Institute of Technology (No. c2007YS0404).

#### References

- 1 F. Cavani, F. Trifiro and A. Vaccari, *Catal. Today*, 1991, **11**, 173–181.
- 2 Y. Zhao, Q. Z. Jiao, C. H. Li and J. Liang, *Carbon*, 2007, **45**, 2159–2163.
- 3 R.H. Baughman, A.A. Zakhidov and W.A. de Heer, *Science*, 2002, **297**, 787–792.
- 4 P. Avouris, *Chem. Phys.*, 2002, **281**, 429–445.
- 5 F. Kreupl, A.P. Graham, G.S. Duesberg, W. Steinhogel, M. Liebau and E. Unger, *Microelectron. Eng.*, 2002, **64**, 399–408.
- 6 P. Serp, M. Corrias and P. Kalck, *Appl. Catal. A: General*, 2003, **253**, 337–358.
- 7 J.H. Bitter, M.K. Van der Lee, A.G.T. Slotboom, A.J. Van Dillen and K.P. de Jong, *Catal. Lett.*, 2003, **89**, 139–142.
- 8 N. Keller, N.I. Maksimova, V.V. Roddatis, M. Schur, G. Mestl and Y.V. Butenko, *Angew. Chem. Int. Ed. Engl.*, 2002, **41**, 1885–1887.
- 9 S. Dommele, K.P. de Jong and J.H. Bitter, *Chem. Commun.*, 2006, 4859–4860.
- 10 C.P. Ewels and M.J. Glerup, *J. Nanosci. Nanotechnol.*, 2005, **5**, 1345–1363.
- 11 M. Terrones, N. Grobert and H. Terrones, *Carbon*, 2002, **40**, 1665–1684.
- 12 N. Hellgren, M.P. Johansson, E. Broitman, L. Hultman and J.E. Sundgren, *Phys. Rev. B*, 1999, **59**, 5162–5169.
- 13 F. Le Normand, J. Hommet, T. Szorenyi, C. Fuchs and E. Fogarassy, *Phys. Rev. B*, 2001, **64**, 235416-1 to 235416-15.
- 14 A.G. Kudashov, A.V. Okotrub, L.G. Bulusheva, I.P. Asanov, Y.V. Shubin and N.F. Yudanov, *J. Phys. Chem. B*, 2004, **108**, 9048–9053.
- 15 H.C. Choi, J. Park and B. Kim, *J. Phys. Chem. B*, 2005, **109**, 4333–4340.
- 16 Y.T. Lee, N.S. Kim, J. Park, J.B. Han, Y.S. Choi and H. Ryu, *Chem. Phys. Lett.*, 2003, **372**, 853–859.
- 17 M. Glerup, M. Castignolles, M. Holzinger, G. Hug, A. Loiseau and P. Bernier, *Chem. Commun.*, 2003, 2542–2543.
- 18 S.Y. Kim, J. Lee, C.W. Na, J. Park, K. Seo and B. Kim, *Chem. Phys. Lett.*, 2005, **413**, 300–305.
- 19 J. Jiang, T. Feng, X. Cheng, L. Dai, G. Cao, B. Jiang, X. Wang, X. Liu and S. Zou, *Nucl. Instrum. Methods Phys. Res., Sect. B*, 2006, **244**, 327–330.
- 20 S. Trasobares, O. Stephan, C. Colliex, W.K. Hsu, H.W. Kroto and D.R.M. Walton, *J. Chem. Phys.*, 2002, **116**, 8966–8972.
- 21 C.C. Tang, Y. Bando, D. Goldberg and F.F. Xu, *Carbon*, 2004, **42**, 2625–2633.
- 22 J. Liu, F. Li, D.G. Evans and X. Duan, *Chem. Commun.*, 2003, 542–543.
- 23 S. Dommele, A. Romero-Izquierdo, R. Brydson, K.P. de Jong and J.H. Bitter, *Carbon*, 2008, **46**, 138–148.
- 24 C.W. Chiou and E.A. Carter, *Surf. Sci.*, 2003, **530**, 87–100.
- 25 Y.T. Lee, N.S. Kim, S.Y. Bae and J. Park, *J. Phys. Chem. B*, 2003, **107**, 12958–12963.